13.5 WIND PROFILE EFFECTS AND CRITICAL LAYER FILTERING OF THE WAVE MOMENTUM FLUX IN STRATIFIED FLOW OVER MOUNTAINS

Miguel A. C. Teixeira* and Pedro M. A. Miranda
CGUL, IDL, University of Lisbon, Lisbon, Portugal

1. INTRODUCTION

The question of how the gravity wave drag produced in stratified flow over mountains is affected by wind profile effects (i.e. shear and curvature) has been the object of recent investigations (Teixeira et. al. 2004, Teixeira and Miranda 2004, 2006). These investigations employed a WKB approximation to treat local impacts on the surface drag of the first and second derivatives of the wind velocity, for generic wind profiles. In order for these effects to be captured, it was necessary to extend the WKB method to 2nd order in the small perturbation parameter, since it was shown that corrections to the surface pressure that are asymmetric with respect to the orography only arise at this order.

While these results have some interest for parameterization purposes, especially when formulated for mountains with an elliptical cross-section (Teixeira and Miranda 2006), the actual force that is exerted on the atmosphere, and therefore directly parameterized, is related with the wave momentum flux. It is the vertical divergence of this momentum flux that produces the reaction force acting on the atmosphere that balances the surface gravity wave drag exerted on the mountain.

By Eliassen-Palm's theorem, and its more recent extension to directional shear flows (Broad 1995), the momentum flux only varies in linear conditions due to the existence of critical levels, where the wave equation is singular. In previous linear studies addressing the momentum flux profiles, wind shear does not have an impact on the surface drag, and the gravity waves are totally absorbed at critical levels (Shutts and Gadian 1999). This occurs because high Richardson numbers (Ri) were considered.

The present study aims to extend this approach to lower Ri, where the surface drag is modified by shear or curvature of the wind profile, and critical levels do not absorb the waves completely, but rather filter them (Teixeira et al 2008). Again, a WKB approximation is employed to obtain the wave solutions for generic wind profiles, but now this method must be extended to 3rd order. The calculations are performed for a circular mountain and tested for three idealized wind profiles with directional shear and constant Ri. Two of these wind profiles are linear, while in the third the wind turns with height at a constant rate, maintaining its magnitude.

Contour integration techniques enable us to obtain simple expressions for the momentum flux, correct to second order in the small perturbation parameter, and closed-form analytical expressions for the momentum flux divergence. The momentum flux profiles are compared with results from numerical simulations, both for linear and weakly nonlinear conditions.

* *Corresponding author address*: Miguel A. C. Teixeira, Centro de Geofísica da Universidade de Lisboa, Edifício C8, Campo Grande, 1749-016 Lisbon, Portugal; e-mail: mateixeira@fc.ul.pt

2. THEORETICAL MODEL

The flow is assumed to be inviscid, non-rotating and hydrostatic, with a constant Brunt Väisälä frequency. If the equations of motion are linearized and combined, the Taylor-Goldstein equation is obtained,

$$\hat{w}'' + \left[\frac{N^2(k^2+l^2)}{(Uk+Vl)^2} - \frac{U''k+V''l}{Uk+Vl} \right] \hat{w} = 0 \,, \qquad (1)$$

where $\hat{w}$ is the Fourier transform of the vertical velocity perturbation, N is the Brunt-Väisälä frequency, $(U(z),V(z))$ is the incoming wind velocity, (k,l) is the horizontal wavenumber of the mountain waves and the primes denote differentiation with respect to height, z. The form assumed for the solution to (1) is

$$\hat{w} = \hat{w}(z=0) e^{\,i\int_0^z \left[m_0(\varepsilon z') + \varepsilon m_1(\varepsilon z') + \varepsilon^2 m_2(\varepsilon z') + \varepsilon^3 m_3(\varepsilon z') \right] dz'} \,, \qquad (2)$$

where the vertical wavenumber m has been expanded in a power series of ε (a small parameter) up to 3rd order. This is necessary for obtaining the momentum flux with sufficient accuracy. When (2) is introduced in (1), four equations result, valid at zeroth, first, second and third order in ε. These equations give definitions for m_0, m_1, m_2, m_3.

Equation (1) is subject to the boundary condition that the flow follows the terrain at the surface,

$$\hat{w}(z=0) = i(U_0 k + V_0 l)\hat{h} \,, \qquad (3)$$

where (U_0,V_0) is the background wind at the surface and $\hat{h}$ is the Fourier transform of the terrain elevation. Additionally, it is required that the wave energy flows upward aloft. This determines the sign of m_0 and m_2.
The definitions of the various terms of the vertical wavenumber are found to be:

$$m_0 = \frac{N(k^2+l^2)^{1/2}}{Uk+Vl} \,, \qquad (4)$$

$$\varepsilon m_1 = -\frac{1}{2} i \frac{U'k+V'l}{Uk+Vl} \,, \qquad (5)$$

$$\varepsilon^2 m_2 = -\frac{1}{8} \frac{(U'k+V'l)^2}{N(k^2+l^2)^{1/2}(Uk+Vl)} - \frac{1}{4} \frac{U''k+V''l}{N(k^2+l^2)^{1/2}} \,, \qquad (6)$$

$$\varepsilon^3 m_3 = -\frac{1}{8} i \frac{(Uk+Vl)(U'''k+V'''l)}{N^2(k^2+l^2)} - \frac{1}{4} i \frac{(U'k+V'l)(U''k+V''l)}{N^2(k^2+l^2)} \,. \qquad (7)$$

This specifies the solution to the mountain wave problem completely.

As mentioned above, the aim of this study is to specify the vertical momentum flux associated with the mountain waves. This momentum flux is given by

$$M_x = -4\pi^2\rho_0 \int_{-\infty}^{+\infty}\int_{-\infty}^{+\infty} \hat{u}^*\hat{w}\, dkdl\,, \qquad (8)$$

$$M_y = -4\pi^2\rho_0 \int_{-\infty}^{+\infty}\int_{-\infty}^{+\infty} \hat{v}^*\hat{w}\, dkdl\,, \qquad (9)$$

respectively for the x and y components, where $\hat{u}$ and $\hat{v}$ are the Fourier transforms of the velocity perturbations along x and y, and ρ_0 is a reference density. These quantities are related to $\hat{w}$ through

$$\hat{u} = \frac{i}{k^2+l^2}\left(ikm - l\frac{V'k - U'l}{Uk+Vl}\right)\hat{w}\,, \qquad (10)$$

$$\hat{v} = \frac{i}{k^2+l^2}\left(ilm + k\frac{V'k - U'l}{Uk+Vl}\right)\hat{w}\,, \qquad (11)$$

where $m=m_0+\varepsilon m_1+\varepsilon^2 m_2+\varepsilon^3 m_3$. Using these equations, and also (2) and (3), and noting that the momentum flux is a real quantity, (8)-(9) may be expressed as:

$$M_x = 4\pi^2\rho_0 \int_{-\infty}^{+\infty}\int_{-\infty}^{+\infty} \frac{k\left|\hat{h}\right|^2}{k^2+l^2}\mathrm{Re}(m)(U_0k+V_0l)^2 e^{-2\mathrm{Im}(s)}\, dkdl\,, \qquad (12)$$

$$M_y = 4\pi^2\rho_0 \int_{-\infty}^{+\infty}\int_{-\infty}^{+\infty} \frac{l\left|\hat{h}\right|^2}{k^2+l^2}\mathrm{Re}(m)(U_0k+V_0l)^2 e^{-2\mathrm{Im}(s)}\, dkdl\,, \qquad (13)$$

where

$$s = \int_0^z m(\varepsilon z')dz'\,. \qquad (14)$$

The determination of s must be carried out separately for the various terms comprising m. m_1 and m_3 may be integrated directly, but the imaginary part of the integral of m_0 and m_2 must be obtained by contour integration. The contour used in the case when $U'k+V'l>0$ at the critical level is shown in Fig. 1. The semi-circles in Fig. 1 are centered on z_c, the critical level height. By design of the wind profiles, it is assumed that the integral along the outer semi-circle is negligible, so the only contribution to the imaginary part of (14) comes from the singularity at z_c. This singularity leads to a discontinuity of the momentum flux contribution from each wavenumber at the critical level. A convenient way to

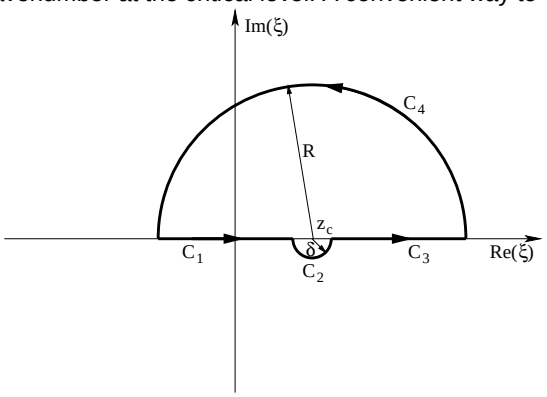

Figure 1. Contour used in the calculation of the integral (14). R is the radius of the outer semi-circle and δ the radius of the inner semi-circle.

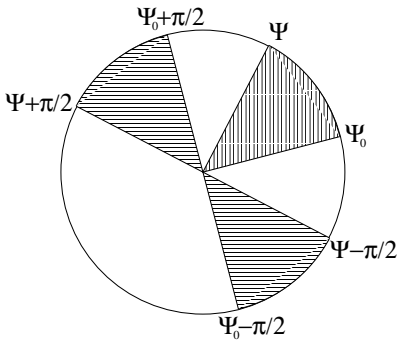

Figure 2. Angles spanned by a generic wind that turns anti-clockwise.(ψ_0 to ψ, vertical hatching) and corresponding angles of the wavenumbers that have been filtered by critical levels (horizontal hatching).

express this effect is by dividing the domain of integration in wavenumber space into two parts: a part where the waves have been filtered by the critical levels and a part where the waves have not been filtered. In Fig. 2, the azimuthal angles of the filtered wavenumbers are denoted by the horizontal hatching.

The momentum flux is normalized by the surface drag in the absence of shear, which is given by

$$D_0 = 4\pi^3\rho_0 N(U_0^2+V_0^2)^{1/2}\int_0^{+\infty}\kappa^2\left|\hat{h}\right|^2 d\kappa\,, \qquad (15)$$

where $\kappa=(k^2+l^2)^{1/2}$. It has been assumed that the mountain that generates the waves is circular, since this makes the normalized momentum flux independent of the detailed shape of the orography.

The final expressions for the normalized momentum flux are:

$$M_x' = \frac{2}{\pi}\left(\int_{\psi-\pi/2}^{\psi_0+\pi/2} I_1\, d\theta + \int_{\psi_0+\pi/2}^{\psi+\pi/2} I_1\cdot I_3\, d\theta\right), \qquad (16)$$

$$M_y' = \frac{2}{\pi}\left(\int_{\psi-\pi/2}^{\psi_0+\pi/2} I_2\, d\theta + \int_{\psi_0+\pi/2}^{\psi+\pi/2} I_2\cdot I_3\, d\theta\right), \qquad (17)$$

where

$$I_1 = \cos\theta\cos(\theta-\psi_0)\left[1-S(\theta,z)\right]\exp\left[S(\theta,z)-S(\theta,0)\right], \qquad (18)$$

$$I_2 = \sin\theta\cos(\theta-\psi_0)\left[1-S(\theta,z)\right]\exp\left[S(\theta,z)-S(\theta,0)\right], \qquad (19)$$

$$I_3 = \exp\left[-2\pi C(\theta)\right], \qquad (20)$$

and

$$S = \frac{1}{8}\frac{(U'\cos\theta+V'\sin\theta)^2}{N^2} + \frac{1}{4}\frac{(U\cos\theta+V\sin\theta)(U''\cos\theta+V''\sin\theta)}{N^2}\,, \qquad (21)$$

$$C = \frac{N}{\left|U_c'\cos+V_c'\sin\theta\right|}\left[1-\frac{1}{8}\frac{(U_c'\cos\theta+V_c'\sin\theta)^2}{N^2}\right], \qquad (22)$$

additionally with $(U_c', V_c')=(U,V)(z=z_c)$.

3. RESULTS

The expressions presented above for the normalized momentum flux will be tested next for three idealized wind profiles with directional shear.

3.1 *Linear wind profile 1*

In the first wind profile considered, the wind varies linearly in the same way as in Shutts and Gadian (1999), i.e.:

$$U = U_0 \, , \; V = \alpha z \, , \tag{23}$$

where U_0>0 and α>0 are constants.

Figure 3 shows momentum flux profiles for Ri=0.5 as a function of dimensionless height $\alpha z/U_0$. The solid line corresponds to the present WKB calculations. The dotted line corresponds to the result of the model of Shutts and Gadian (1999), developed for high Ri. The dashed line corresponds to the WKB model modified to take into account the finite horizontal dimensions of the numerical integration domain. The filled symbols denote numerical simulations carried out in very nearly linear conditions, and the open symbols numerical simulations for Nh_0/U_0=0.5 (see Teixeira and Miranda 2008 for details). As can be seen, the best agreement with the linear numerical results is achieved by the limited-area WKB model. The results using Shutts and Gadian's (1999) model clearly produce worse agreement everywhere. The nonlinear numerical simulations show that the drag is enhanced by nonlinear processes (the corresponding symbols are only presented for $\alpha z/U_0$>0.7 due to the presence of the mountain).

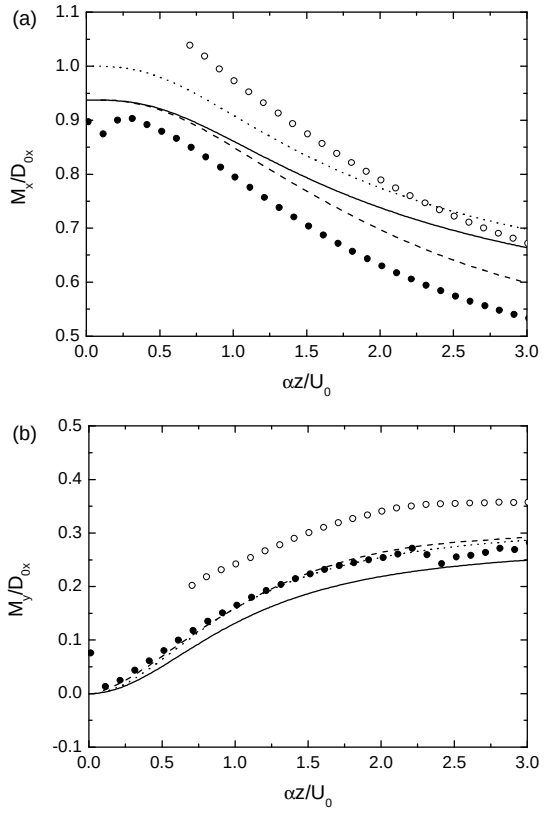

Figure 3. Normalized momentum flux as a function of normalized height for Ri=0.5. Dotted line: Shutts and Gadian (1999), Solid line: WKB infinite-area model, dashed line: WKB limited-area model, filled symbols: linear numerical simulation, open symbols: numerical simulation for Nh_0/U_0=0.5. (a) *x* component, (b) *y* component.

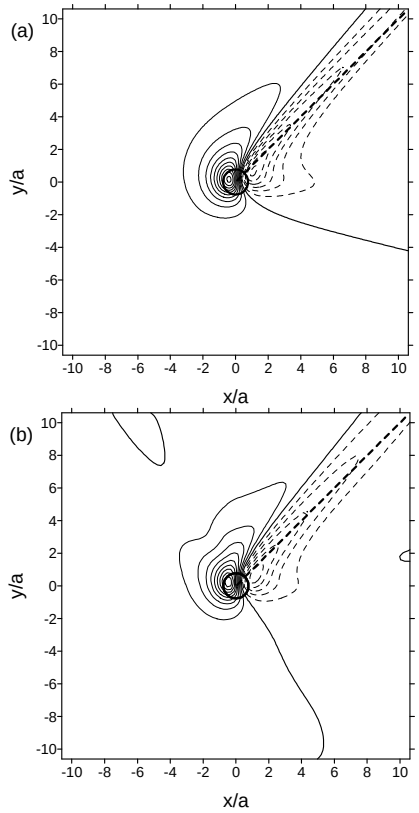

Figure 4. Normalized isentropic surface vertical displacement for the linear simulations of Fig. 3 at a normalized height $\alpha z/U_0$=1. Solid lines: positive, dashed lines: negative. (a) WKB model, (b) numerical model.

Figure 5 shows the vertical displacement of isentropic surfaces for the linear case of Fig. 3, at a height $\alpha z/U_0$=1, from the WKB model and from numerical simulations. The agreement is quite good, namely the number of contours is similar and the shape of the pattern only differs slightly. There is an elongated 'tail' in the fields shown in Fig. 4 along the direction of the mean wind at the displayed height (thick dashed line). This is due to the filtering effect of the critical level.

3.2 *Linear wind profile 2*

The second linear wind profile to be considered is similar to one of those adopted by Teixeira et al. (2004):

$$U = U_0 - \alpha z \, , \; V = U_0 \, , \tag{24}$$

where, again, U_0>0 and α>0 are constants. There is considerably more wind rotation for this profile than for the previous one, leading to more substantial momentum flux variation with height.

Figure 5 shows the momentum flux profiles, as a function of dimensionless height $\alpha z/|\mathbf{U}_0|$ for Ri=0.5. Again, the best agreement with the linear numerical

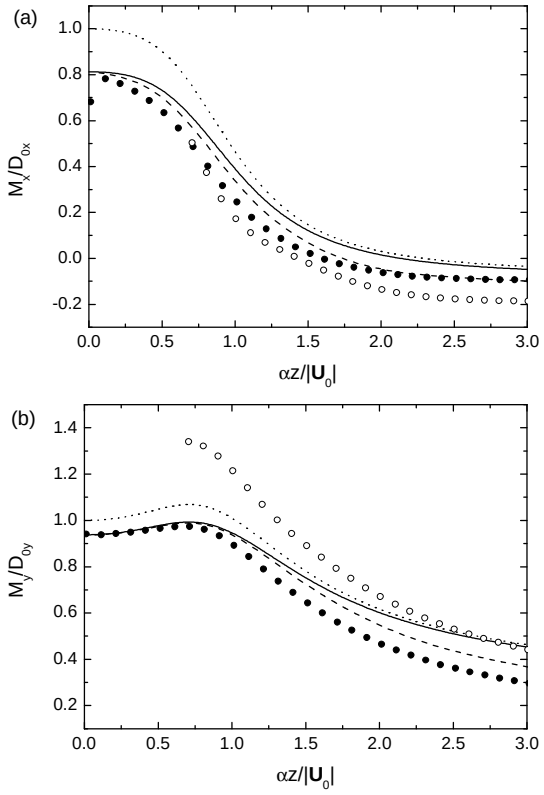

Figure 5. As Fig. 3, but for the linear wind profile 2.

results is achieved by the limited-area WKB model. The infinite-area WKB model overestimates the momentum flux slightly, especially at larger heights, while the model of Shutts and Gadian (1999) overestimates it more severely, and especially near the surface. Nonlinear results show, again, a momentum flux enhancement for the *y* component, but a decrease in magnitude for the *x* component. This is probably related with the fact that the *x* momentum flux component changes sign as height increases.

Figure 6 shows the vertical displacement of isentropic surfaces for the linear case of Fig. 5, at a height $\alpha z/|\mathbf{U}_0|=1$, from the WKB model and from the numerical simulations. There is a reasonable degree of

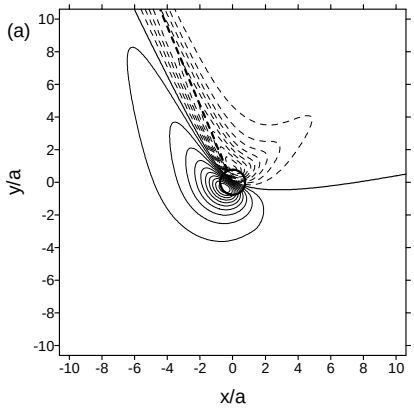

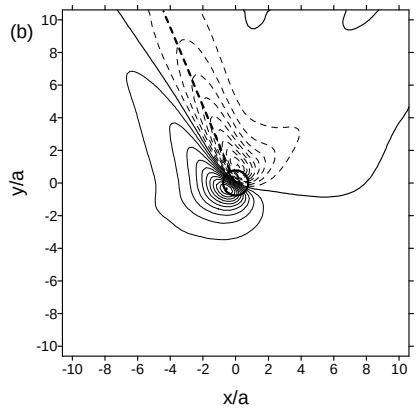

Figure 6. As Fig. 4, but for the linear wind profile 2, and $\alpha z/|\mathbf{U}_0|=1$.

agreement, but in the numerical simulations the 'tail' in the field which exists along the wind direction is considerably more spread laterally than in the analytical result. This is probably a result of spurious diffusion, due to the finite resolution of the numerical simulations.

3.3 *Wind that turns with height*

The third and final wind profile to be considered corresponds to a wind that turns with height maintaining its magnitude (cf. Teixeira et al. 2004),

$$U = U_0 \cos(\beta z)\,,\; V = U_0 \sin(\beta z)\,, \qquad (25)$$

where $U_0>0$ and $\beta>0$ are constants.

In Fig. 7, the momentum flux can be seen as a function of normalized height $\beta z/\pi$. Since the surface drag is larger than for a linear wind profile (increasing as Ri decreases and therefore being larger than its value without shear), the momentum flux predicted by the WKB model is also larger than that predicted by the model of Shutts and Gadian (1999). The *x* component is in quite good agreement (either for an infinite area of for a limited area) with the linear numerical simulations, except near the surface, where it somewhat underestimates the numerical results. At $\beta z/\pi=1$, where the wind has turned by an angle of π, all wavenumbers in the wave spectrum have been filtered by critical levels. This leads the *x* momentum flux to become slightly negative. This feature is also well-captured by

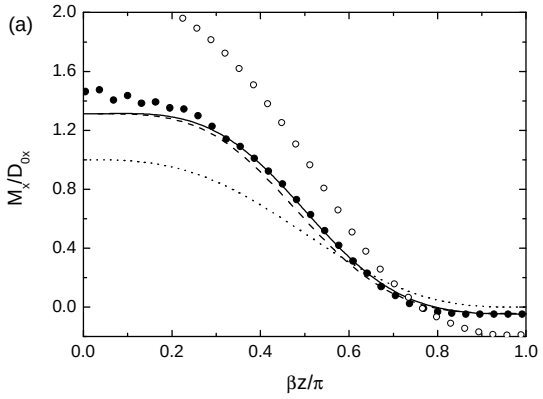

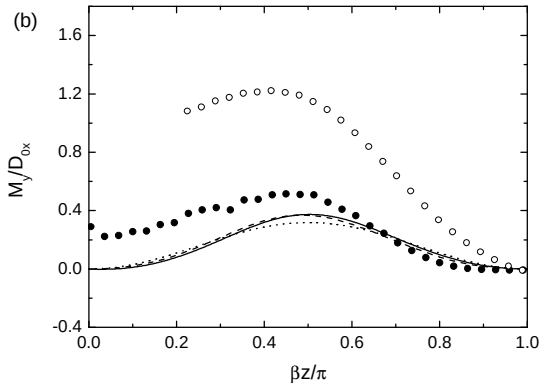

Figure 7. As Fig. 3, but for a wind that turns with height.

the WKB model.

In the nonlinear numerical runs, the momentum flux increases considerably, and the agreement with the WKB model is not good, but clearly the WKB model provides a large improvement upon Shutts and Gadian's (1999) model, which underestimates the *x* momentum flux much more severely. The prediction of the *y* component of the momentum flux is rather worse, with the analytical models being in particular unable to capture its non-zero value at the surface. This problem is inherent to the WKB approximation.

In Fig. 8, the vertical displacement of isentropic surfaces is shown at the height $\beta z/\pi=1/3$. Again, there is some resemblance between the analytical and the numerical results, although not as close as, for example, in Fig. 4.

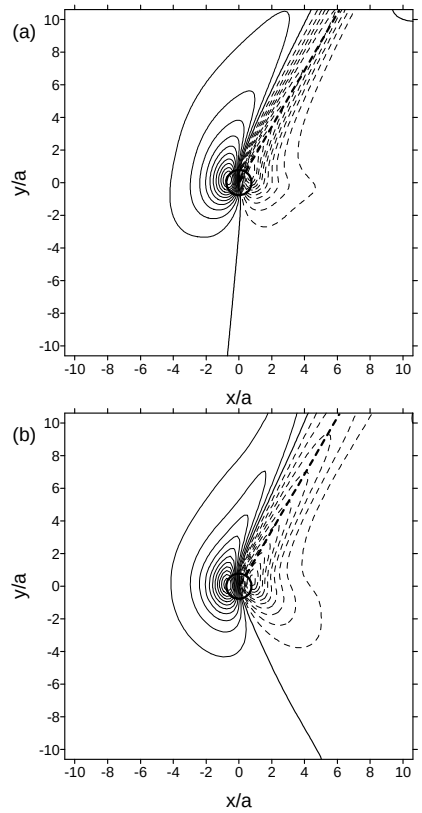

Figure 8. As Fig. 4, but for a wind that turns with height, and $\beta z/\pi=1/3$.

4. CONCLUDING REMARKS

Momentum flux profiles accurate to second order in a small perturbation parameter were calculated using a 3rd order WKB approximation, for stratified flows with directional shear over a circular mountain. These calculations complement those presented by Teixeira et al. (2004) for the surface mountain wave drag. The explicit form of the momentum flux expressions was obtained through contour integration methods, and is given in terms of simple 1D integrals. The momentum flux divergence (which corresponds to the drag force acting on the atmosphere) can be provided in closed analytical form (not shown).

The momentum fluxes obtained from the WKB model were compared, for three idealized wind profiles, with the results of numerical simulations, in linear and weakly nonlinear conditions. The WKB model considerably improves the predictions of the model of Shutts and Gadian (1999) (developed for high Ri), for Ri as low as 0.5, especially when the finite horizontal extent of the domain is taken into account. In nonlinear conditions, the momentum fluxes are amplified somewhat, and differ more from the theoretical predictions. However, they remain closer to the results of the improved model presented here than to results of previous models.

Acknowledgements

This work was funded by FCT under project AWARE/PTDC/CTE-ATM/65125/2006.

5. REFERENCES

Broad, A. S., 1995: Linear theory of momentum fluxes in 3-D flows with turning of the mean wind with height. *Quart. J. Roy. Meteor. Soc.*, **121**, 1891-1902.

Shutts, G. J. and Gadian, A., 1999: Numerical simulations of orographic gravity waves in flows which back with height. *Quart. J. Roy. Meteor. Soc.*, **125**, 2743-2765.

Teixeira, M. A. C. and Miranda, P. M. A., 2004: The effect of wind shear and curvature on the gravity wave drag produced by a ridge. *J. Atmos. Sci.*, **61**, 2638-2643.

Teixeira, M. A. C. and Miranda, P. M. A., 2006: A linear model of gravity wave drag for hydrostatic sheared flow over an alliptical mountain. *Quart. J. Roy. Meteor. Soc.*, **132**, 2439-2458.

Teixeira, M. A. C. and Miranda, P. M. A., 2008: On the momentum fluxes associated with mountain waves in directionally sheared flows. Submitted to *Quart. J. Roy. Meteor. Soc.*

Teixeira, M. A. C., Miranda, P. M. A. and Argaín, J. L., 2008: Mountain waves in two-layer sheared flows: critical-level effects, wave reflection and drag enhancement. *J. Atmos. Sci.*, **65**, 1912-1926.

Teixeira, M. A. C., Miranda, P. M. A. and Valente, M. A. 2004: An analytical model of mountain wave drag for wind profiles with shear and curvature. *J. Atmos. Sci.*, **61**, 1040-1054.